Desalination and Water Treatment
www.deswater.com
doi: 10.5004/dwt.2020.25082

180 (2020) 309–316
March

Phosphate recovery from wastewater using sludge-derived carbon as uranium decontaminant

Huimin Zhang, Qingying Zheng, Aiping Chen, Jianyou Long, Diyun Chen, Lingjun Kong*

Guangdong Provincial Key Laboratory of Radionuclides Pollution Control and Resources, Rural Non-point Source Pollution Comprehensive Management Technology Center of Guangdong Province, School of Environmental Science and Engineering, Guangzhou University, Guangzhou 510006, China, Tel. +86-02039366942; emails: kongljun@gzhu.edu.cn (L. Kong), zhm08285520@163.com (H. Zhang), 13719132877@163.com (Q. Zheng), 15521226534@163.com (A. Chen), longjyou@gzhu.edu.cn (J. Long), cdy@gzhu.edu.cn (D. Chen)

Received 23 May 2019; Accepted 23 October 2019

ABSTRACT

Carbonization of sludge into biochar as adsorbents in application of wastewater decontamination was widely concerned to address the issues of sludge resource utilization and wastewater treatment. Herein, sewage sludge was carbonized at various temperatures to obtain biochar (SC) for phosphate removal, further being considered as a uranium decontaminant. Batch adsorption experiments were conducted to investigate the adsorption kinetics and isotherms of SC to phosphate. Results showed that the pseudo-second-order kinetic model and Langmuir model fitted well to the adsorption kinetic and isotherm results, respectively. Adsorption of phosphate on the SCs was ascribed to monolayer chemical adsorption process. The SC obtained at 800°C (SC-800) had the highest adsorption capacity of 13.89 mg/g to K_3PO_4. The adsorption mechanism was regarded as the mineralization of the phosphate with Ca element in the SC to form $Ca(H_2PO_4)_2$ and $CaH_2P_2O_5$ crystals. The $Ca(H_2PO_4)_2$ and $CaH_2P_2O_5$ crystals performed prefer uranium adsorption ability to SC-800. The formation of nanoflakes confirmed the favorable uranium adsorption due to the presence of $Ca(H_2PO_4)_2$ and $CaH_2P_2O_5$ crystals after phosphate adsorption. Thus, the recovered phosphate on SC-800 could be a promising uranium decontaminant.

Keywords: Sewage sludge; Biochar; Phosphate; Adsorption; Uranium

1. Introduction

Phosphorus (P) is an indispensable and irreplaceable non-renewable resource for human life and industrial production [1], while the consumption of phosphorus resource in the world is on the rise. At the same time, a large amount of phosphorus-containing water is discharged into the water environment at present. Once the concentration of phosphorus exceeds the phosphorus standard of 0.02 mg/L, it accelerates eutrophication of surface water body, which causes serious harm to water environment and human health [2]. To avoid the crisis of phosphorus resource loss and water environment hazard, more attention is being urgently paid to the treatment of phosphate wastewater and the recovery of phosphorus resource.

Until now, methods such as biological treatment [3], chemical precipitation [4], adsorption [5] have been widely concerned on P-containing wastewater treatment. Among them, biological method requires a large processing structure and rigorous operation condition while lots of chemical sludge are generated from chemical precipitation method. Fortunately, adsorption method has attracted much attention in wastewater decontamination due to its high efficiency, simple operation, and free secondary pollution. More

* Corresponding author.

importantly, the resource could be extracted after adsorption, which could address the advantages of resource recovery from pollutants decontamination. The suitable adsorbent is key for adsorption.

A wide variety of adsorbents have been used for phosphate removing. Natural minerals (zeolite [6], diatomite [7], bentonite [8]), whose main chemical components are metal oxides or oxygen-containing functional groups, can be used as efficient adsorbents. It is well known that conversion of solid waste into adsorbents greatly concerned the issues of sustainable development and ecological civilization construction. Industrial wastes (slag [9], red mud [10–12], fly ash [13,14]) containing a large amount of metal oxides can be converted into adsorbents to address the view of waste utilization. Activated carbon [15], usually prepared from coal [16], shell [17] and sawdust [18], can be used to adsorb phosphate due to its large specific surface area and porous structure.

Sludge, as a by-product of wastewater treatment, was inevitably generated during wastewater treatment. Disposal and treatment of the sludges are widely concerned since they are intractable at present due to the large quantities and harmful environmental impact. Carbonizing the sludge into biochar could greatly reduce the amount of sludge and stabilize the pollutants such as pathogenic bacteria and heavy metals in sludge. As early as 1971, the sewage sludge was carbonized into biochar to prepare cheap biochar adsorbents [19]. Fortunately, pathogenic bacteria were destructed and the heavy metals were incorporated into the graphite crystals of SC. Since then, sludge had attracted attention as an adsorbent [20]. It is reviewed from literatures that sludge derived adsorbents were widely concerned on the treatment of volatile organic gas pollutants [21], NO_x [22], H_2S [23], heavy metals [24] and organic pollutants [25], and so on. Further activation was required to enhance the BET surface area. Whether the sludge carbon without activation could be an efficient decontaminant? It was interestingly reported that the calcium and iron-modified biochar performed favorable ability to phosphate adsorption from aqueous solution [26–28]. Since the inorganic elements were concentrated in biochar in the presence of microwave-assisted pyrolysis [29], the sludge char with concentrated calcium, aluminium minerals obtained from carbonization may be promising for phosphate adsorption; thus, the phosphate could be recovered and enriched in the sludge char. It is inspiring and promising for reuse of the phosphate-enriched sludge char.

Since the uranium-containing wastewater was generated increasingly with the rapid development of nuclear industry and the overexploitation of uranium, various nanoparticles were explored for uranium decontamination [30]. Interestingly, the hydroxyapatite was reported for uranium decontamination in our previous study [31,32]; thus, the recovered phosphate was hypothesized to be a decontaminant for uranium removing.

In this work, sewage sludge was converted into biochar at various carbonization temperatures. The obtained SC is hypothesized to be efficient for enriching phosphate, further the enriched phosphate could be reused for uranium decontamination. The phosphate removal performance was studied by isothermal adsorption model and kinetic model. The product after phosphate adsorption is analyzed by X-ray powder diffractometer (XRD) analysis. More importantly, the recovered phosphate was confirmed to be efficient for uranium decontamination, which is important to understand the resource utilization of sludge, the treatment of phosphorus and uranium-containing wastewater.

2. Materials and methods

2.1. Materials

The dewatered sludge was obtained from the Datansha wastewater treatment plant. The sludge was dried and dehydrated at 105°C, then was crushed and sieved through 100 meshes. Potassium orthophosphate (K_3PO_4), dipotassium hydrogen phosphate (K_2HPO_4) and monopotassium phosphate (KH_2PO_4) are analytical grades, being purchased from Sigma Chemical Reagent Co., Ltd. K_3PO_4, K_2HPO_4 and KH_2PO_4 in a concentration of 1,000 mg/L were prepared as stock solution. U (VI) stock solution (C_0 = 1,000 mg/L) was prepared by dissolving a predetermined mass of uranyl nitrate ($UO_2(NO_3)_2{\cdot}6H_2O$) (GR) in 0.1 mol/L of nitric acid, further being diluted to 1 L and a pH of 3.

2.2. Preparation of sludge biochar

40 g of dry sludge powder was placed in the ceramic ark. Next, the sample was placed in the quartz glass tube of the programmable tubular resistance furnace. The nitrogen in a flow of 100 mL/min was involved to sweep the air in the quartz tube for 30 min. After that, the tube furnace was heated to 500°C, held for 120 min and cooled to room temperature. The sample was washed repeatedly until the pH in solution was around 7. Finally, it was filtered, dried, ground, and sieved through 100 meshes sieve, being recorded as SC-500. Similarly, an appropriate amount of dry sludge was carbonized at 600°C, 700°C, 800°C as described above. The obtained materials were recorded as SC-600, SC-700, SC-800 corresponding to the carbonization temperature.

2.3. Batch adsorption experiments

The resulted SC was put into the PO_4^{3-}–P-containing solution in a dosage of 3 g/L, being placed in a conical flask and shaken in a water bath oscillator. At each predetermined time interval, the sample was extracted and filtered by 0.45 μm filter membrane to remove the adsorbents. The concentration of residual phosphate was measured by molybdenum antimony spectrophotometry [33], and the adsorption amount of phosphate was calculated by the difference of phosphate concentration in solution before and after adsorption. The adsorption amounts were calculated by Eq. (1) as follows:

$$q_t = \frac{C_0 - C_t}{m} \times V \tag{1}$$

where C_0 and C_t (mg/L) are phosphate concentration at initial and t time, respectively; V is the volume of adsorbate (L); m is the mass of adsorbent (g).

For the isotherm study, the adsorbents were added into a series of PO_4^{3-}–P-containing solutions with various initial concentrations (10–200 mg/L) at a dosage of 3 g/L. Afterwards,

the flasks were put in a water bath oscillator shaken at 200 rpm for 240 min. Next, the suspension was taken out and filtrated to measure the residual PO_4^{3-}–P concentration. The SC-800 after K_3PO_4 adsorption was named as SC-800-K_3PO_4. The adsorption capacity (q_e, mg/g) at equilibrium was calculated by Eq. (2):

$$q_e = \frac{C_0 - C_e}{m} \times V \quad (2)$$

where C_0 and C_e are the initial and equilibrium concentration (mg/L); V and m were described above.

In the case of uranium adsorption experiments, first, 0.01 g of SC-800 and SC-800-K_3PO_4 were added into a series of 10 mL of U (VI) solution in various concentrations. Furthermore, they were shaken in a water batch oscillator at 30°C and 200 rpm for 1 h to equilibrium. 5 M sodium hydroxide and sulfuric acid were used to adjust the solution pH value to 3.0. The suspension was filtrated using a glass syringe equipped with a 0.45 μm syringe filter to remove the solid particles. The residual U (VI) concentration was analyzed using a uranium photo-electric meter (WGJ-III, DAJI photo-electric Co., Hangzhou, China). The adsorption capacity was calculated as described above.

All the adsorption experiments were repeated three times. The average value of each experiment and error was calculated.

2.4. Analytical methods

The BET specific surface area of the biochar was determined by using a physisorption apparatus (SA 3100, Beckman Coulter, USA). The samples were subjected to infrared spectrum analysis using a Fourier transform infrared spectrometer (FTIR, Tensor27, Bruker, Germany). The phase of the sample before and after adsorption was analyzed by an XRD (PW3040/60, Holland).

3. Results and discussion

3.1. Characterization of SC

Table 1 presents the XRF analysis of sludge. Obviously, aluminium, silica, calcium and iron-containing minerals were presented in the sludge. These minerals may be in favor of phosphate adsorption because the calcium decorated sludge carbon accelerated the phosphate adsorption [27]. Thus, the calcium was concentrated after carbonization. The calcium-containing mineral may favor the phosphate adsorption.

The specific surface area is one of the important factors affecting the adsorption ability of biochar. Table 2 shows that the specific surface areas of SC-500, SC-600, SC-700 and SC-800 increased with the increase in carbonization temperature, which were 20.65, 70.89, 124.32 and 132.56 m^2/g, respectively. It suggested that the carbonization temperature played a positive effect on increasing the specific surface area of biochar due to the release of volatile organic gas during carbonization process [34]. The results were confirmed by the SEM analysis as shown in Fig. 1. More cracks were observed

Table 1
Element content in the sludge and SC-800 analyzed by XRF (mass %)

Sample	Sludge
Mg	1.32
Al	13.5
Si	25.2
P	6.62
S	2.83
K	3.24
Ca	8.01
Ti	5.04
Cr	1.54
Mn	1.00
Fe	28.9

Table 2
Effect of carbonized temperature on the surface area of the biochar (m^2/g)

Adsorbent	BET (m^2/g)
SC-500	20.65
SC-600	70.89
SC-700	124.32
SC-800	132.56

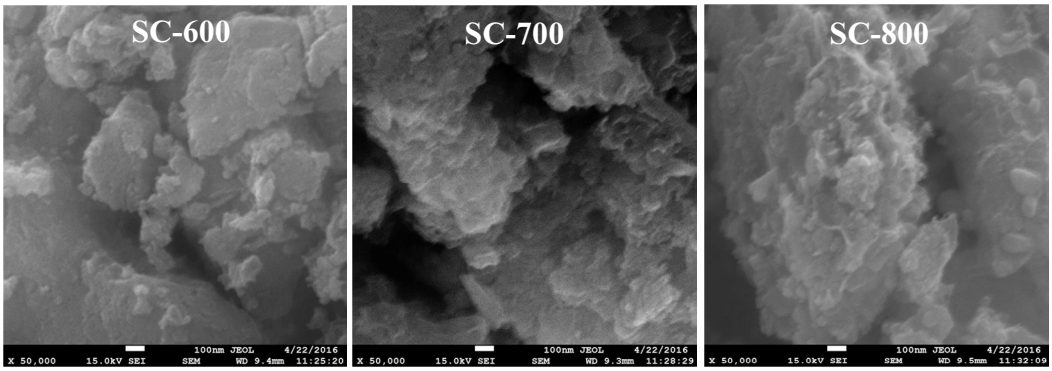

Fig. 1. SEM analysis of the SC-600, SC-700 and SC-800.

on the surfaces of SC-700 and SC-800 comparing with that on SC-600. In addition, the difference in specific surface area between SC-700 and SC-800 is indistinguishable. The result could be explained by the fact that release of organic volatile was similar during carbonization at 700°C and 800°C.

3.2. Phosphate adsorption studies

A yellow substance was observed in the solution when the SC-500 was conducted as adsorbent for P removal, indicating that sludge carbonization at 500°C is insufficient and its properties are unstable. In this case, SC-500 will not be used in the subsequent adsorption experiments. Fortunately, the yellow substance was not observed for SC-600, SC-700 and SC-800, adsorption of P on them were investigated in the following experiments. Fig. 2 presents the adsorption capacities of P as a function of contact time. Obviously, the adsorption capacities increased rapidly within the initial 20 min, further being increased to equilibrium slowly after about 200 min. The rapid adsorption of P on SCs could be ascribed to the surface adsorption of P on SCs. After that, internal diffusion contributed to the adsorption of P on SCs, which is time dependent. SC-700 and SC-800 had the adsorption capacities of 7.5 and 7.44 mg/g to P, they were higher than that of 6.99 mg/g for SC-600.

The pseudo-first-order and pseudo-second-order kinetic models were given in Eqs. (3) and (4), respectively, to illustrate the adsorption kinetics of P on SCs. The corresponding kinetic parameters are shown in Table 3.

$$q_t = q_e\left(1 - e^{-k_1 t}\right) \tag{3}$$

$$\frac{t}{q_t} = \frac{t}{q_e} + \frac{1}{k_2 q_e^2} \tag{4}$$

where q_e and q_t are the adsorption amount at equilibrium and at time t, respectively. k_1 and k_2 are subject to pseudo-first-order and pseudo-second-order kinetic rate constants, respectively.

The correlation coefficients calculated from the pseudo-second-order kinetic model were greater than 0.98 as shown in Table 3, indicating that the pseudo-second-order kinetic model fitted well with the adsorption kinetics of biochar to P in aqueous. The adsorption process can be considered as chemical adsorption [35]. The order of adsorption rate is SC-600 < SC-700 < SC-800, which is in agreement with the specific surface area. It is clear that carbonization can improve its adsorption performance of P from aqueous solution.

The adsorption capacities of phosphate on SCs were investigated by the adsorption equilibrium isotherm studies. Fig. 3 displays the well-known nonlinear fitting curves of the Langmuir and Freundlich isotherm adsorption models, which are presented in Eqs. (5) and (6):

$$q_e = \frac{q_{\max} K_L C_e}{1 + K_L C_e} \tag{5}$$

$$q_e = K_F C_e^{\frac{1}{n}} \tag{6}$$

where q_e and C_e are the equilibrium adsorption capacity and concentration, respectively; $q_{\max}$ is the saturated adsorption capacity; K_L is the constant of surface adsorption strength. The parameter of K_F describes the adsorption density under standard conditions. The parameter of n indicates the binding energy distribution on the surface [36].

As illustrated in Fig. 3, the adsorption behaviors of the three biochars (SC-600, SC-700, SC-800) to phosphate was better fitted with the Langmuir model compared with the Freundlich model. The correlation coefficients (R^2) were 0.992, 0.991 and 0.993 for Langmuir models, while the correlation coefficients were 0.964, 0.959, 0.961 for Freundlich models as shown in Table 4. The relatively higher correlation coefficients confirmed the well-fitted Langmuir model. The corresponding maximum adsorption capacities of SC-600,

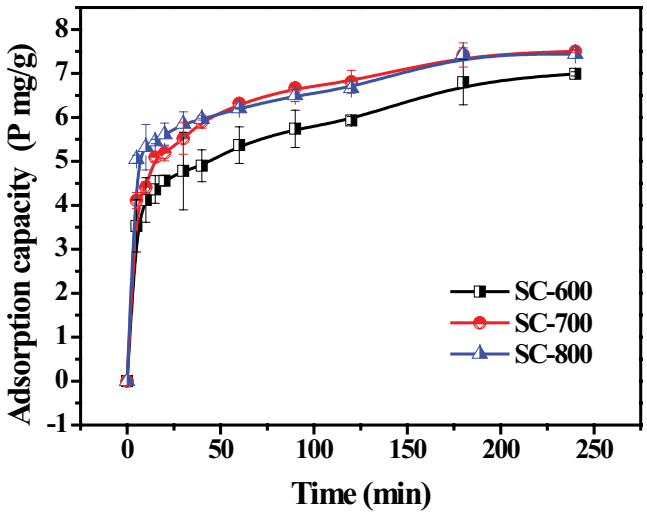

Fig. 2. Change in the adsorption amount of phosphate as a function of time.

Table 3
Adsorption kinetic parameters of phosphate on the SCs

Adsorbents	Pseudo-first-order kinetics		Pseudo-second-order kinetics		
	k_1 (min^{-1})	R^2	k_2 (g/(mg min))	q_e (mg/g)	R^2
SC-600	0.0157	0.943	0.0124	7.0621	0.990
SC-700	0.0135	0.977	0.0155	7.6336	0.996
SC-800	0.0166	0.883	0.0190	7.5131	0.995

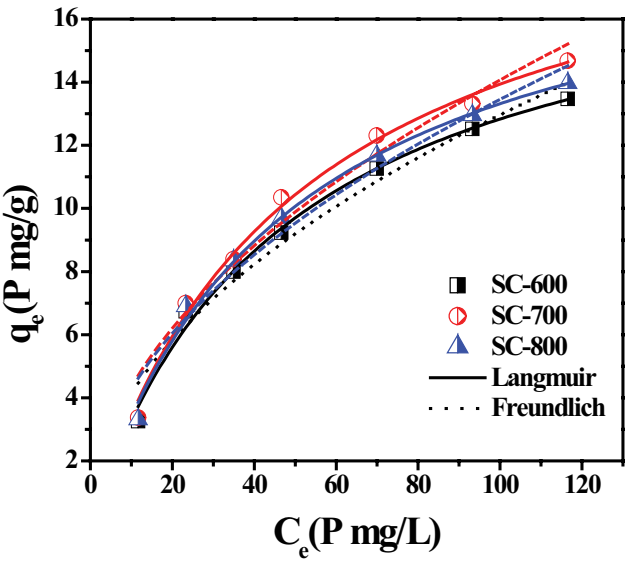

Fig. 3. Langmuir and Freundlich models fitted adsorption equilibrium isotherms of phosphate on the SC-600, SC-700, SC-800.

SC-700, SC-800 were 18.95, 20.98 and 19.69 mg/g, respectively, which were consistent with the BET surface area of the SCs (SC-700 > SC-800 > SC-600).

The Langmuir adsorption model is based on the following assumptions: (1) adsorption is limited to monolayer; (2) all surface sites are equivalent; (3) the adsorption site is independent of the occupancy rate of adjacent sites [37]. It can be concluded that the adsorption of phosphate on biochar belongs to the surface monolayer adsorption. Moreover, the dimensionless constant separation factor R_L can be used to represent the basic characteristics of the Langmuir isotherm, as described in Eq. (7) [38]:

$$R_L = \frac{1}{1 + K_L C_0} \tag{7}$$

where C_0 indicates the initial concentration of the adsorbate (mg/L), K_L is the Langmuir constant (L/mg). R_L represents the affinity of adsorption, that is, $0 < R_L < 1$ for favorable adsorption, $R_L > 1$ for unfavorable adsorption, $R_L = 1$ for reversible adsorption; and $R_L = 0$ for irreversible adsorption [38]. The obtained R_L value, which ranged from 0 to 1 (Table 4), indicated that adsorption of P on the sludge biochar was favorable.

Since the species of phosphate are related to the pH value of the solution, the adsorption capacities of SC-800 for KH_2PO_4, K_2HPO_4 and K_3PO_4 are displayed in Table 5. Biochar had the greatest adsorption capacity of 13.89 mg/g for K_3PO_4 at the dosage of 3 g/L, while they were 9.86 and 7.06 mg/g for K_2HPO_4 and KH_2PO_4, respectively. It indicates that the adsorption process is ascribed to the chemisorptions between the adsorbent and PO_4^{3-}.

To further evaluate the adsorption capacity of P on SCs, the maximum adsorption capacities of various adsorbents for P reported in the literature were shown in Table 6. Carbon-based materials were widely used as adsorbents due to their high surface area. Sewage sludge carbon had the maximum adsorption capacities of 2.77 mg/g for phosphate [39]. However, natural zeolites exhibited poor adsorption capacity of phosphate due to low affinity [40–42]. Subsequently, a series of zeolite composites were prepared to increase the adsorption ability to phosphate. Zirconium-modified zeolite (ZrMZ) [43], nano Z–Al (aluminum zeolite) [40], NaOH-activated and lanthanum-impregnated zeolite (NLZ) were synthesized to adsorb phosphate [44]. All of them exhibited better adsorption ability to phosphate, and the maximum adsorption capacities were 5.96, 7.0 and 8.96 mg/g, respectively. Further, adsorption ability could be enhanced by metal ions decoration. Mg–Al hydrotalcite-loaded kaolin clay (MKC) had a maximum adsorption capacity of 11.85 mg/g as shown in Table 5 [45]. In this work, the excess sludge carbonized at 800°C showed a considerable adsorption capacity of 19.69 mg/g to phosphate, owing to the interaction of Ca in sludge carbon and phosphate in the solution.

3.3. Characterization of adsorption products

To explore the adsorption mechanism of biochar to phosphate, Fig. 4 shows the XRD patterns of SC-800 and SC-800 after adsorption of KH_2PO_4, K_3PO_4, respectively. It can be seen that two distinct diffraction peaks appeared

Table 5
Comparison of adsorption ability of SC-800 to phosphates in varied form

	KH_2PO_4	K_2HPO_4	K_3PO_4
pH[a]	6.56	8.23	10.69
pH[b]	8.39	9.58	10.65
Q_e (mg/g)	7.06	9.86	13.89

[a]pH before adsorption.
[b]pH after adsorption.

Table 4
Fitted isotherm adsorption parameters of biochar for K_3PO_4

Samples	Langmuir				Freundlich		
	q_{max} (mg/g)	K_L(L/mg)	R_L	R^2	K_F (mg^{-1})(L mg^{-1})$^{1/n}$	1/n	R^2
SC-600	18.95	0.021	0.713	0.992	1.321	0.496	0.964
SC-700	20.98	0.020	0.701	0.991	1.349	0.509	0.959
SC-800	19.69	0.021	0.712	0.993	1.363	0.497	0.961

Table 6
Comparison of the maximum adsorption capacities of reported adsorbents to phosphate

Adsorbents	Surface area (m^2/g)	C_0 (mg/L)	pH	Q_{max} (mg/g)	References
SC-800	132.56	20	Unadjusted	19.69	This work
SAC	218.37	5	5	2.77	[39]
ZrMZ	71.83	3	7	5.96	[43]
Z-Al	–	25	7	7.0	[40]
NLZ	–	5	7	8.96	[44]
MKC	23.57	50	7.5	11.85	[45]

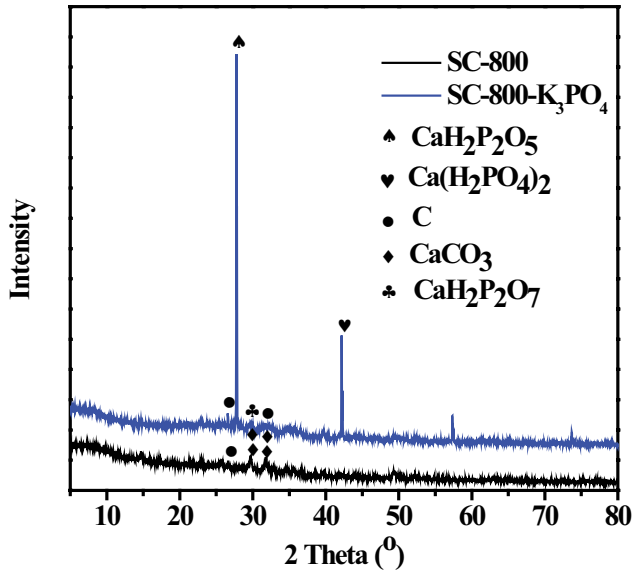

Fig. 4. XRD spectra of the SC-800 and SC-800 after adsorption of phosphate.

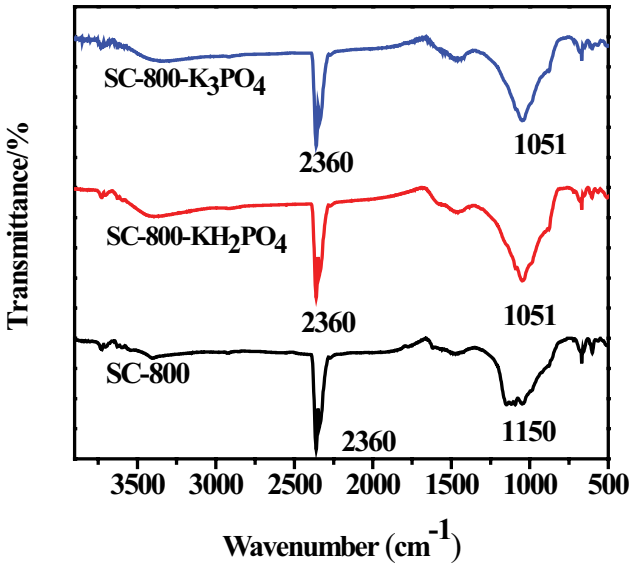

Fig. 5. FT-IR spectra of the SC-800 and SC-800 after adsorption of phosphates.

near at 27.25° and 42.17° after adsorption of K_3PO_4 on SC-800. Through the PDF card search analysis, the two peaks were assigned to $CaH_2P_2O_5$ (PDF#36-0002) and $Ca(H_2PO_4)_2$ (PDF#09-0390), respectively. The results showed that element Ca in sludge contributed to the phosphate adsorption except for Fe, Si, etc. The Ca can react with K_3PO_4 to form two crystalline products of $CaH_2P_2O_5$ and $Ca(H_2PO_4)_2$. In addition, the diffraction peak of $CaH_2P_2O_5$ was higher and sharper, indicating that $CaH_2P_2O_5$ exhibits high crystallinity. Moreover, desorption of phosphate was not observed in the aqueous solution of pH 7, confirming that the formed products of $CaH_2P_2O_5$ and $Ca(H_2PO_4)_2$ were stable. Therefore, the Ca element contained in the SC-800 can react with K_3PO_4 to form a crystal mineral to recover the phosphate from wastewater.

Fig. 5 showed the FT-IR spectrum of SC-800 before and after adsorption of KH_2PO_4 and K_3PO_4, respectively. The spectra after adsorption were almost identical. The difference between the spectra before and after adsorption was mainly reflected at around 1,150 cm^{-1}. The maximum absorption peak before adsorption occurred at around 1,150 cm^{-1} to about 1,400 cm^{-1}. The absorption peak was mainly vibrational peaks of C–O, C=C and C=O, and the absorption peaks were mainly telescopic carboxylic acids, carbonates, aromatic rings and amides. Since sludge was used as a raw material in this work, the decomposition of organic matter contained therein will produce C=C and C=O. After adsorption of KH_2PO_4 and K_3PO_4 on SC-800, the P=O characteristic peak of 1,300 cm^{-1} was transferred to about 1,051 cm^{-1}, and the position of 1,200 cm^{-1} in the original sludge carbon was changed. In summary, KH_2PO_4 and K_3PO_4 could be adsorbed on the SCs.

3.4. Application of the recovered phosphate as uranium decontaminant

Since the $CaH_2P_2O_5$ and $Ca(H_2PO_4)_2$ were the main products after phosphate recovery, they were considered as uranium decontaminant due to that the hydroxyapatite was reported for uranium adsorption in our previous study [31,32]. Fig. 6 presented a comparison of the uranium adsorption on SC-800 and SC-800-K_3PO_4 at various initial concentration. Clearly, the removal efficiency of uranium on SC-800 was 99.9%, and the adsorption capacity was 9.99 mg/g when the uranium initial concentration was 10 mg/L, but the removal efficiency decreased to 82.7% as the initial concentration

increased to 20 mg/L. Interestingly, the adsorption capacity of uranium on SC-800-K_3PO_4 was 19.98 mg/g when the uranium initial concentration was 20 mg/L. The uranium adsorption capacity on SC-800-K_3PO_4 was quite higher than that on SC-800 when the initial concentration increased to 20 mg/L. Because the phosphate was determined in SC-800, it was easy to understand that the SC-800 could adsorb the uranium from aqueous solution, thus the nano-flakes were formed after uranium adsorption as shown in the inset (a) in Fig. 6, the nano-flakes were similar with the uranium adsorbed on the recovered hydroxyapatite reported in our previous work [46]. While the phosphate was adsorbed on SC-800, the uranium adsorption capacity on SC-800-K_3PO_4 was highly increased as described above, nano-flakes were also observed as shown in the inset (b) in Fig. 6. $CaH_2P_2O_5$ and $Ca(H_2PO_4)_2$ were observed on SC-800-K_3PO_4 after phosphate adsorption on SC-800, the favorable uranium adsorption on SC-800-K_3PO_4 was ascribed to the interaction of uranium with $CaH_2P_2O_5$ and $Ca(H_2PO_4)_2$, further nano-flakes were also formed [32]. Thus, the SC-800 could be a promising decontaminant for phosphate adsorption and further for uranium adsorption.

4. Conclusions

The excess sludge can be converted into biochar by carbonization at different temperatures and used to remove phosphate from wastewater. SC-800 performed the highest adsorption capacity and rate to phosphate. The pseudo-second-order kinetic model and Langmuir model could describe the adsorption behavior of phosphate on SC-800 well. Monolayer adsorption contributed to the phosphate adsorption on SC-800, which is a favorable adsorption process. Among the KH_2PO_4, K_2HPO_4 and K_3PO_4, SC-800 exhibited the highest adsorption capacity for K_3PO_4. $CaH_2P_2O_5$ and $Ca(H_2PO_4)_2$ crystals were the fate of phosphate being adsorbed on SC due to the reaction of Ca in the sludge carbon with PO_4^{3-}. Furthermore, the SC-800-K_3PO_4 could be promising for uranium decontamination due to the presence of $CaH_2P_2O_5$ and $Ca(H_2PO_4)_2$. Thus, the sewage sludge could be converted into a promising decontaminant for recycling phosphate and removing uranium from aqueous solution.

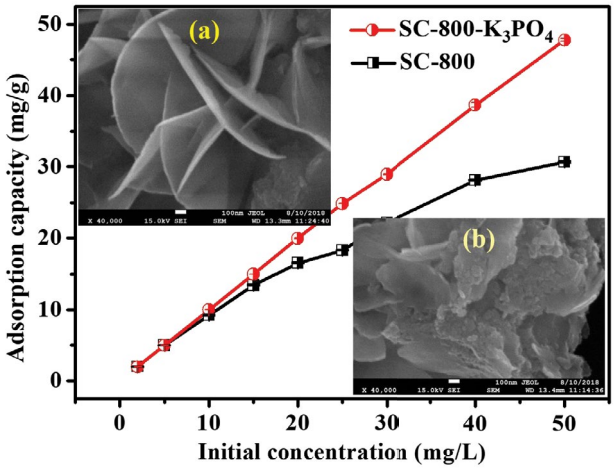

Fig. 6. Application of the SC-800 and SC-800-K_3PO_4 for uranium adsorption with a dosage of 1.00 g/L (inset: SEM of them (a) before and (b) after uranium adsorption).

Acknowledgments

This work was supported by the National Natural Science Foundation of China (21976042, U1501231), The Project of Guangdong Provincial Key Laboratory of radioactive contamination control and resources (2017B030314182); Natural Science Foundation of Guangdong Provincial (2016A030 310265), the Science and Technology Research Programs of Guangzhou City (201607010311), University's 2017 Training Program for Young Top-Notch Personnel (BJ201706), Project supported by Guangdong Province Universities and Colleges Pearl River Scholar Funded Scheme, 2018.

References

[1] S.G. Barbosa, L. Peixoto, B. Meulman, M.M. Alves, M.A. Pereira, A design of experiments to assess phosphorous removal and crystal properties in struvite precipitation of source separated urine using different Mg sources, Chem. Eng. J., 298 (2016) 146–153.
[2] C.L. Schelske, Eutrophication: focus on phosphorus, Science, 324 (2009) 722–722.
[3] W. Cai, W.L. Huang, Z.F. Lei, Z.Y. Zhang, D.O. Lee, Y. Adachi, Granulation of activated sludge using butyrate and valerate as additional carbon source and granular phosphorus removal capacity during wastewater treatment, Bioresour. Technol., 282 (2019) 269–274.
[4] X. Lu, K. Shih, X.Y. Li, G. Liu, E. Zeng, F. Wang, Accuracy and application of quantitative x-ray diffraction on the precipitation of struvite product, Water Res., 90 (2016) 9–14.
[5] F. Xie, F. Wu, G. Liu, Y. Mu, C. Feng, H. Wang, J. Giesy, Removal of phosphate from eutrophic lakes through adsorption by in situ formation of magnesium hydroxide from diatomite, Environ. Sci. Technol., 48 (2014) 582–590.
[6] N. Karapınar, Application of natural zeolite for phosphorus and ammonium removal from aqueous solutions, J. Hazard. Mater., 170 (2009) 1186–1191.
[7] J. Chen, L. Yan, H. Yu, S. Li, L. Qin, G. Liu, Y. Li, B. Du, Efficient removal of phosphate by facile prepared magnetic diatomite and illite clay from aqueous solution, Chem. Eng. J., 287 (2016) 162–172.
[8] M. Zamparas, A. Gianni, P. Stathi, Y. Deligiannakis, I. Zacharias, Removal of phosphate from natural waters using innovative modified bentonites, Appl. Clay Sci., 62–63 (2012) 101–106.
[9] C. Barca, C. Gérente, D. Meyer, F. Chazarenca, Y. Andrès, Phosphate removal from synthetic and real wastewater using steel slags produced in Europe, Water Res., 46 (2012) 2376–2384.
[10] C. Liu, Y. Li, Z. Luan, Z. Chen, H. Zhang, Z. Jia, Adsorption removal of phosphate from aqueous solution by active red mud, J. Environ. Sci., 19 (2007) 1166–1170.
[11] Y. Zhao, J. Wang, Z. Luan, X. Peng, Z. Liang, L. Shi, Removal of phosphate from aqueous solution by red mud using a factorial design, J. Hazard. Mater., 165 (2009) 1193–1199.
[12] S. Prajapati, P. Najar, V. Tangde, Removal of phosphate using red mud: an environmentally hazardous waste by-product of alumina industry, Adv. Phys. Chem., 2 (2016) 1–9.
[13] S. Lu, S. Bai, L. Zhu, H.D. Shan, Removal mechanism of phosphate from aqueous solution by fly ash, J. Hazard. Mater., 161 (2009) 95–101.
[14] K. Xu, T. Deng, J. Liu, W. Peng, Study on the phosphate removal from aqueous solution using modified fly ash, Fuel, 89 (2010) 3668–3674.
[15] Z. Shi, F. Liu, S. Yao, Adsorptive removal of phosphate from aqueous solutions using activated carbon loaded with Fe(iii) oxide, New Carbon Mater., 26 (2011) 299–306.

[16] S. Asaoka, T. Yamamoto, Characteristics of phosphate adsorption onto granulated coal ash in seawater, Mar. Pollut. Bull., 60 (2010) 1188–1192.
[17] S. Yeom, K. Jung, Recycling wasted scallop shell as an adsorbent for the removal of phosphate, J. Ind. Eng. Chem., 15 (2009) 40–44.
[18] M. Unnithan, V. Vinod, T. Anirudhan, Ability of iron(iii)-loaded carboxylated polyacrylamide-grafted sawdust to remove phosphate ions from aqueous solution and fertilizer industry wastewater: adsorption kinetics and isotherm studies, J. Appl. Polym. Sci., 84 (2002) 2541–2553.
[19] F.N. Kemmer, S.R. Robertson, R.D. Mattix, Sewage Treatment Process. Naclo Chemical Company, U.S. Patent. No. (1971) 3,619,420.
[20] Z. Li, N. Jiang, F. Wu, Z. Zhou, Experimental investigation of phosphorus adsorption capacity of the waterworks sludges from five cities in China, Ecol. Eng., 53 (2013) 165–172.
[21] L.J. Kong, Y. Xiong, S.H. Tian, R. Luo, C. He, H. Huang, Preparation and characterization of a hierarchical porous char from sewage sludge with superior adsorption capacity for toluene by a new two-step pore-fabricating process, Bioresour. Technol., 146 (2013) 457–462.
[22] R. Pietrzak, T.J. Bandosz, Activated carbons modified with sewage sludgederived phase and their application in the process of NO_2 removal, Carbon, 45 (2007) 2537–2546.
[23] T.J. Bandosz, K.A. Block, Removal of hydrogen sulfide on composite sewage sludge-industrial sludge-based adsorbents, Ind. Eng. Chem. Res., 45 (2006) 3666–3672.
[24] F. Rozada, M. Otero, A. Morán, A.I. García, Adsorption of heavy metals onto sewage sludge-derived materials, Bioresour. Technol., 99 (2008) 6332–6338.
[25] L.J. Kong, Y. Xiong, L.P. Sun, S.H. Tian, R.B. Xu, C.Y. Zhao, R.S. Luo, X. Yang, K. Shih, H.Y. Liu, Sorption performance and mechanism of a sludge-derived char as porous carbon-based hybrid adsorbent for benzene derivatives in aqueous solution, J. Hazard. Mater., 274 (2014) 205–211.
[26] S.D. Wang, L.J. Kong, J.Y. Long, M.H. Su, Z.H. Diao, X.Y. Chang, D.Y. Chen, G. Song, K. Shih, Adsorption of phosphorus by calcium-flour biochar: Isotherm, kinetic and transformation studies, Chemosphere, 195 (2018) 666–672.
[27] L.J. Kong, M.N. Han, K. Shih, M.H. Su, Z.H. Diao, J.Y. Long, Chen, D.Y. Chen, L. Hou, Y. Peng, Nano-rod Ca-decorated sludge derived carbon for removal of phosphorus, Environ. Pollut., 233 (2018) 698–705.
[28] L.J. Kong, X. Hu, Z. Xie, X. Ren, J. Long, M. Su, Z. Diao, D. Chen, K. Shih, L. Hou, Accelerated phosphorus recovery from aqueous solution onto decorated sewage sludge carbon, Sci. Rep., 8 (2018) 13421.
[29] E. Antunes, J. Schumann, G. Brodie, M.V. Jacob, P.A. Schneider, Biochar produced from biosolids using a single-mode microwave: characterisation and its potential for phosphorus removal, J. Environ. Manage., 196 (2017) 119–126.
[30] X.X. Wang, L. Chen, L. Wang, Q.H. Fan, D.Q. Pan, J.X. Li, F.T. Chi, Y. Xie, S.J. Yu, C.L. Xiao, F. Luo, J. Wang, X.L. Wang, C.L. Chen, W.S. Wu, W.Q. Shi, S. Wang, X.K. Wang, Synthesis of novel nanomaterials and their application in efficient removal of radionuclides, Sci. China-Chem., 62 (2019) 933–967.
[31] L. Kong, H. Zhang, W. Ji, K. Shih, M. Su, Z. Diao, R. Xu, L. Hou, G. Song, D. Chen, Recovery of phosphorus rich krill shell biowaste for uranium immobilization: A study of sorption behavior, surface reaction, and phase transformation, Environ. Pollut., 243 (2018) 630–636.
[32] M. Han, L.J. Kong, X. Hu, D. Chen, X. Xiong, H. Zhang, M. Su, Z. Diao, Y. Ruan, Phase migration and transformation of uranium in mineralized immobilization by wasted biohydroxyapatite, J. Clean. Prod., 197 (2018) 886–894.
[33] Y. Zhan, H. Zhang, J. Lin, Z. Zhang, J. Gao, Role of zeolite's exchangeable cations in phosphate adsorption onto zirconium-modified zeolite, J. Mol. Liq., 243 (2017) 627–637.
[34] A. Jain, R. Balasubramanian, M. Srinivasan, Hydrothermal conversion of biomass waste to activated carbon with high porosity: a review, Chem. Eng. J., 283 (2016) 789–805.
[35] W.P. Xiong, Z.T. Zeng, X. Li, G.M. Zeng, R. Xiao, Z.H. Yang, Y.Y. Zhou, C. Zhang, M. Cheng, L. Hu, C.Y. Zhou, L. Qin, R. Xu, Y.R. Zhang, Multi-walled carbon nanotube/amino-functionalized MIL-53(Fe) composites: remarkable adsorptive removal of antibiotics from aqueous solutions, Chemosphere, 210 (2018) 1061–1069.
[36] S.A. Zhong, C.Y. Zhou, X.N. Zhang, H. Zhou, H. Li, X.H. Zhu, Y. Wang, A novel molecularly imprinted material based on magnetic halloysite nanotubes for rapid enrichment of 2,4-dichlorophenoxyacetic acid in water, J. Hazard. Mater., 276 (2014) 58–65.
[37] C.Y. Zhou, H. Li, H. Zhou, H. Wang, P.J. Yang, S. Zhong, Water-compatible halloysite-imprinted polymer by Pickering emulsion polymerization for the selective recognition of herbicides, J. Sep. Sci., 38 (2015) 1365–1371.
[38] S.J. Allen, G. Mckay, K.Y.H. Khader, Equilibrium adsorption isotherms for basic dyes onto lignite, J. Chem. Technol. Biotechnol., 45 (2010) 291–302.
[39] S. Yao, M. Wang, J. Liu, S. Tang, Removal of phosphate from aqueous solution by sewage sludge-based activated carbon loaded with pyrolusite, J. Water Reuse Desal., 8 (2018) 192–201.
[40] D. Guaya, C. Valderrama, A. Farran, C. Armijos, J.L. Cortina, Simultaneous phosphate and ammonium removal from aqueous solution by a hydrated aluminum oxide modified natural zeolite, Chem. Eng. J., 271 (2015) 204–213.
[41] J. Hrenovic, M. Rozic, L. Sekovanic, A. Anic-Vucinic, Interaction of surfactant-modified zeolites and phosphate accumulating bacteria, J. Hazard. Mater., 156 (2008) 576–582.
[42] P. Ning, H. Bart, B. Li, X. Lu, Y. Zhang, Phosphate removal from wastewater by model-La (III) zeolite adsorbents, J. Environ. Sci., 20 (2008) 670–674.
[43] J. Lin, Z. Zhang, Y. Zhan, Effect of humic acid preloading on phosphate adsorption onto zirconium-modified zeolite, Environ. Sci. Pollut. Res., 24 (2017) 12195–12211.
[44] Y. He, H. Lin, Y. Dong, Q. Liu, L. Wang, Simultaneous removal of ammonium and phosphate by alkaline-activated and lanthanum-impregnated zeolite, Chemosphere, 164 (2016) 387–395.
[45] L. Deng, Z. Shi, Synthesis and characterization of a novel Mg–Al hydrotalcite-loaded kaolin clay and its adsorption properties for phosphate in aqueous solution, J. Alloys Compd., 637 (2015) 188–196.
[46] L.J. Kong, Y. Ruan, Q.Y. Zheng, M.H. Su, Z.H. Diao, D.Y. Chen, L. Hou, X.Y. Chang, K. Shih, Uranium extraction using hydroxyapatite recovered from phosphorus containing wastewater, J. Hazard. Mater., 382 https://doi.org/10.1016/j.jhazmat.2019.120784.